

Two- and three-point functions in two-dimensional Landau-gauge Yang-Mills theory: Continuum results

Markus Q. Huber,^a Axel Maas,^b Lorenz von Smekal^a

^a*Institut für Kernphysik, Technische Universität Darmstadt, Schlossgartenstr. 2, 64289 Darmstadt, Germany*

^b*Institute for Theoretical Physics, Friedrich-Schiller-University Jena, Max-Wien-Platz 1, D-07743 Jena, Germany*

E-mail: markus.huber@physik.tu-darmstadt.de, axel.maas@uni-jena.de,
lorenz.smekal@physik.tu-darmstadt.de

ABSTRACT: We investigate the Dyson-Schwinger equations for the gluon and ghost propagators and the ghost-gluon vertex of Landau-gauge gluodynamics in two dimensions. While this simplifies some aspects of the calculations as compared to three and four dimensions, new complications arise due to a mixing of different momentum regimes. As a result, the solutions for the propagators are more sensitive to changes in the three-point functions and the ansätze used for them at the leading order in a vertex expansion. Here, we therefore go beyond this common truncation by including the ghost-gluon vertex self-consistently for the first time, while using models for the three-gluon vertex which reproduce the known infrared asymptotics and the zeros at intermediate momenta as observed on the lattice. A separate computation of the three-gluon vertex from the results is used to confirm the stability of this behavior a posteriori. We also present further arguments for the absence of the decoupling solution in two dimensions. Finally, we show how in general the infrared exponent κ of the scaling solutions in two, three and four dimensions can be changed by allowing an angle dependence and thus an essential singularity of the ghost-gluon vertex in the infrared.

KEYWORDS: Green functions, Yang-Mills theory, two dimensional quantum field theory, infrared behavior

1 Introduction

Quantum chromodynamics (QCD) is the theory of quarks and gluons. It is well understood in the perturbative regime, but phenomena like confinement and chiral symmetry breaking are intrinsically non-perturbative and their investigation therefore requires adequate methods. Some of these effects are believed to be present already for the gluonic sector alone, i. e., Yang-Mills theory, on which we will focus here. One approach to understand the non-perturbative properties is based on the correlation functions, which are also used as input in many phenomenological applications. However, correlation functions are in general gauge-dependent.

A common gauge choice is the Landau gauge, for which propagators and vertices have been calculated with several methods, see, for instance, [1–25], summarized in the recent review [26]. For various reasons investigations were extended from four also to three [3, 4, 18, 27–30] and two dimensions [3, 4, 28, 31–34]. One of the main motivations for this is that lattice calculations become much cheaper in lower dimensions so one can more easily reach low momenta. An approach complementary to lattice calculations is based on functional equations [35] like functional renormalization group equations, see, e. g., [36–39], or Dyson-Schwinger equations (DSEs), see, e. g., [26, 40–45], for which large scale separations are less problematic. However, since they consist of an infinite tower of equations, truncations are required.

The situation in four dimensions is interesting, because with continuum methods one finds two types of solutions, while lattice methods yield only one. The two types are called decoupling and scaling solutions. The former [11, 13, 16, 17, 20, 21] is characterized by a gluon propagator that becomes finite at zero momentum while the ghost propagator behaves like a massless particle. On the other hand, the scaling solution [1–4, 20, 21] features an infrared (IR) vanishing gluon propagator and an IR enhanced ghost propagator. On the lattice only the decoupling type of solution is seen in four and three dimensions. Currently there does not exist a consensus in the community if only one solution is physical or both types are valid and possibly correspond to different non-perturbative completions of the Landau gauge, see [26] for a compilation of the current state of affairs. The situation in three dimensions is essentially the same.

On the other hand, the two dimensional case is different: Lattice calculations [31, 33] seem not to find the decoupling type solution, but the results resemble more the scaling type solution. However, studies in the strong coupling limit show that the situation is not completely clear, since the analytically known scaling relation for the IR exponents is not fulfilled for $\beta = 0$ and the coupling does not become a constant [46]. The results for the dressing functions at finite β fit reasonably well with results from analytic analyses using functional methods [3, 4, 28, 34], but an agreement between the IR exponents extracted from the lattice data [31, 33, 46, 47] is not reached. Results obtained within the Gribov-Zwanziger framework [32] corroborate the non-existence of the decoupling type solution as does Ref. [34]. In the latter also a bound on the gluon propagator at zero momentum incompatible with this type of solution was derived.

In the present work we want to extend the currently available analytic results from DSEs in two dimensions [3, 4, 28, 34] and present the first solutions at all momenta. We confirm the absence of the decoupling solution from Dyson-Schwinger equations in agreement with lattice and prior results also when taking the full momentum range into account. Although the underlying equations seem easier to solve in two dimensions than in four dimensions, for example, because no renormalization has to be performed, we find that they have their own intricacies. The reason is that in two dimensions different momentum regions influence each other. Especially the mid-momentum behavior, which is where the truncations of DSEs are most influential, is very important in order to obtain correct results. This can

be uniquely traced back to the subtle cancellations required for the scaling solution in two dimensions. As a consequence, it is non-trivial in two dimensions to find a viable truncation which works over the whole momentum range for the deep infrared to the ultraviolet. As a result we will discuss several model ansätze for the vertices. As a final step we also include the ghost-gluon vertex to the set of equations to be solved numerically. In this system of equations the only undetermined quantity is the three-gluon vertex, which we adjust such as to obtain the correct ghost UV behavior.

We will explain the setup of the equations and fix our notation in Sec. 2. Then we will consider the ghost DSE numerically in Sec. 3. In Sec. 4 we present analytic results and the coupled system of the propagators DSEs is investigated numerically in Sec. 5. In Sec. 6 we present the results of the system of propagators and ghost-gluon vertex. We conclude with a summary in Sec. 7. Two appendices contain details on the integral kernels and results for the three-gluon vertex.

2 Dyson-Schwinger equations of two-dimensional Yang-Mills theory

The Euclidean Lagrangian of Yang-Mills theory fixed to the Landau gauge reads

$$\mathcal{L} = \frac{1}{4} F_{\mu\nu}^a F_{\mu\nu}^a + \frac{1}{2\xi} (\partial A^a)^2 - \bar{c}^a M^{ab} c^b, \quad (2.1)$$

where $F_{\mu\nu}^a$ is a component of the field strength tensor $F_{\mu\nu} = F_{\mu\nu}^a T^a$ with the Hermitian generators T^a of the gauge group and M^{ab} is the Faddeev-Popov operator:

$$F_{\mu\nu}^a := \partial_\mu A_\nu^a - \partial_\nu A_\mu^a + i g f^{abc} A_\mu^b A_\nu^c, \quad (2.2)$$

$$M^{ab} := -\delta^{ab} \partial^2 - g f^{abc} \partial_\mu A_\mu^c. \quad (2.3)$$

The DSEs can be derived from this Lagrangian with standard methods, see, for example, [40, 42, 44]. Since vertex DSEs are already rather complex the program *DoFun* [44, 48] was used for their derivation.

The propagators of the ghost and gluon fields are given by

$$D_{gh}(p^2) := -\frac{G(p^2)}{p^2}, \quad D_{gl}(p^2) := P_{\mu\nu}(p) \frac{Z(p^2)}{p^2}, \quad (2.4)$$

respectively, where the transverse projector is $P_{\mu\nu}(p) = \delta_{\mu\nu} - p_\mu p_\nu / p^2$. Their full DSEs are given in Fig. 1. In the IR we will use the parametrization

$$G^{IR}(p^2) = B \cdot (p^2)^{\delta_{gh}}, \quad Z^{IR}(p^2) = A \cdot (p^2)^{\delta_{gl}} \quad (2.5)$$

for the dressing functions, where δ_{gh} and δ_{gl} are the so-called IR exponents which describe the IR behavior of the dressings qualitatively. For the scaling solution they are related by [3, 4]

$$2\delta_{gh} + \delta_{gl} = \frac{(4-d)}{2}. \quad (2.6)$$

Consequently, in the case of the scaling solution the IR behavior of both dressing functions can be described by one variable only which we will denote by $\kappa := -\delta_{gh}$.

For the two-point DSEs we adopt a standard truncation scheme from four dimensions where all diagrams involving the bare four-gluon vertex are dropped. Such a truncation conserves the leading IR and UV behavior. In order to obtain a scalar equation from the gluon DSE we project it with the

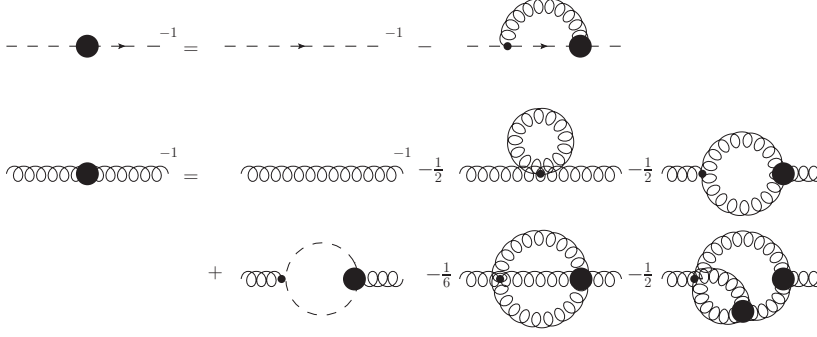


Figure 1. Full two-point Dyson-Schwinger equations of Landau gauge Yang-Mills theory. All internal propagators are dressed. Thick blobs denote dressed vertices. Wiggly lines are gluons, dashed ones ghosts.

transverse projector, yielding

$$\frac{1}{G(p^2)} = 1 + N_c g^2 \int_q Z(q^2) G((p+q)^2) K_G(p, q) \Gamma^{A\bar{c}c}(q; p+q, p) \quad (2.7)$$

$$\begin{aligned} \frac{1}{Z(p^2)} &= 1 + N_c g^2 \int_q G(q^2) G((p+q)^2) K_Z^{gh}(p, q) \Gamma^{A\bar{c}c}(p; p+q, q) \\ &\quad + N_c g^2 \int_q Z(q^2) Z((p+q)^2) K_Z^{gl}(p, q) \Gamma^{A^3}(p, q, p+q). \end{aligned} \quad (2.8)$$

The quantities $\Gamma^{A\bar{c}c}$ and Γ^{A^3} are dressing functions of the ghost-gluon and three-gluon vertices, respectively, and \int_q stands for $\int d^2q/(2\pi)^2$. The kernels K_G , K_Z^{gh} and K_Z^{gl} are given explicitly in Appendix A.

The dressed ghost-gluon vertex is described by two dressing functions

$$\Gamma_\mu^{A\bar{c}c, abc}(k; p, q) := i g f^{abc} (P_{\mu\nu}(k) p_\nu D_t^{A\bar{c}c}(k; p, q) + k_\mu D_l^{A\bar{c}c}(k; p, q)). \quad (2.9)$$

The basis tensors have been chosen such that $D_t^{A\bar{c}c}(k; p, q)$ and $D_l^{A\bar{c}c}(k; p, q)$ are the purely transverse and longitudinal dressing functions, respectively. After transverse projection then only $D_t^{A\bar{c}c}(k; p, q)$ contributes and $\Gamma^{A\bar{c}c}(k; p, q)$ from eqs. (2.7) and (2.8) can be identified with $D_t^{A\bar{c}c}(k; p, q)$.¹ The bare vertex is $i g f^{abc} p_\mu$.

The three-gluon vertex has in general 14 Lorentz tensors. Only four of them are transverse and thus contributing in the Landau gauge. Furthermore we only consider the color antisymmetric part. As part of our truncation we only take into account the tree-level tensor:

$$\Gamma_{\mu\nu\rho}^{A^3, abc}(p, q, r) = i g f^{abc} (g_{\mu\nu}(q-p)_\rho + g_{\nu\rho}(r-q)_\mu + g_{\rho\mu}(p-r)_\nu) D^{A^3}(p, q, r). \quad (2.10)$$

Thus $\Gamma^{A^3}(p, q, r)$ in eqs. (2.7) and (2.8) is identical to $D^{A^3}(p, q, r)$.

Specific expressions for the dressing functions of the vertices will be given below.

¹In the notation of [4] we have $D_t^{A\bar{c}c}(k; p, q) = A(k; p, q)$ and $D_l^{A\bar{c}c}(k; p, q) = B(k; p, q) + A(k; p, q) p \cdot k / k^2$.

3 The ghost Dyson-Schwinger equation

This DSE is the simplest one because it has only one integral with a relative simple structure (compared to the gluon loop of the gluon DSE) and is automatically UV finite. Consequently it is in general relatively easy to study numerically using input for the gluon propagator and the ghost-gluon vertex, see, for example, [16]. In the two-dimensional case the ghost DSE provides additional important information. First we investigate the existence of various types of solutions, then the influence of the mid-momentum regime on the UV behavior of the ghost propagator is scrutinized. In this section we use a bare ghost-gluon vertex and various ansätze for the gluon dressing function.

3.1 Existence of decoupling and scaling solutions

In functional equations the choice between decoupling or scaling solutions is realized via the ghost Dyson-Schwinger equation. Employing the subtracted DSE,

$$\frac{1}{G(p^2)} - \frac{1}{G(p_0^2)} = \int_q Z(q^2)G((p+q)^2)K_G(p,q)\Gamma^{A\bar{c}c}(q;p+q,p) - \int_q Z(q^2)G((p_0+q)^2)K_G(p_0,q)\Gamma^{A\bar{c}c}(q;p_0+q,p_0), \quad (3.1)$$

we have to specify the value of the ghost dressing function at p_0 . Most conveniently one may choose $p_0 = 0$. For a finite value of $1/G(0)$ a decoupling solution is obtained, whereas a scaling solution corresponds to $1/G(0) = 0$. When solving the coupled system of the two-point DSEs the gluon propagator then automatically becomes of the decoupling or scaling type in four dimensions [2, 4, 21].

The unsubtracted ghost DSE in two dimensions was considered in Ref. [34], where it was found that in order to avoid IR divergences at $p^2 = 0$ the gluon propagator has to vanish at zero momentum. Here we will corroborate these results numerically. Therefor we use various ansätze for the gluon dressing function, which are depicted in Fig. 2:

$$Z_{ans}(p^2) = \frac{1}{4} \left(\frac{1}{p^2 + 1} \right)^2 (p^2)^{\delta_{gl}} + \left(\frac{p^2}{p^2 + 1} \right)^2 \frac{1}{1 + 1/p^2} + \frac{1}{2} c_{gl} \frac{p^4}{10 + p^6}. \quad (3.2)$$

For now the parameter c_{gl} is set to one. The IRE exponent δ_{gl} is either 1 for the decoupling type ansatz or 1.4 for the scaling type ansatz.

The subtracted ghost DSE in Eq. (3.1) was solved using a standard fixed point iteration. The resulting ghost propagator dressing functions are shown in figs. 3 and 4. For the scaling type ansatz the expected power law is perfectly obeyed in the IR, while for the decoupling type ansatz no valid solution is found. First of all the obtained ghost dressing function, depicted in Fig. 4, does not become constant in the IR but diverges. Fitting the IR exponent locally, i. e., extracting the IR exponent from two adjacent points, shows that the exponent does not settle to a constant value but keeps decreasing slowly. Secondly the ghost dressing depends on the value of the used IR cutoff, as shown in Fig. 4, hinting at the occurrence of IR divergences. Trying several variations of the gluon dressing function ansatz could not remove this problem as expected from the analytic considerations of Ref. [34]. For the scaling type solution the results for the same IR cutoffs as used for the decoupling type solution lie on top of each other.

Note that both the analytic [34] and the numeric arguments are based on the assumption that the ghost-gluon vertex is constant in the IR and does not deviate much from the tree-level at intermediate momenta. From lattice calculations alone, however, we can strictly speaking not infer that for a decoupling solution, because what we see there seems to be a scaling solution. Also the often cited

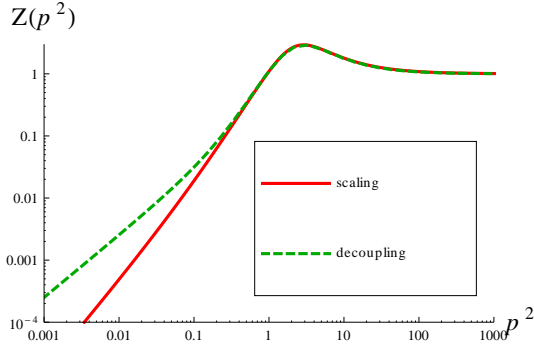


Figure 2. Input gluon propagator dressing functions of decoupling and scaling types from Eq. (3.2) with $c_{gl} = 1$ and $\kappa = 1$ (decoupling) and $\kappa = 1.4$ (scaling). This plot and the following were created with *Mathematica* [49]

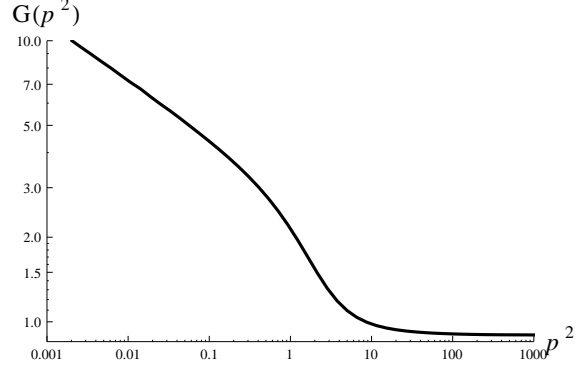


Figure 3. Ghost propagator dressing function resulting from the scaling type gluon propagator.

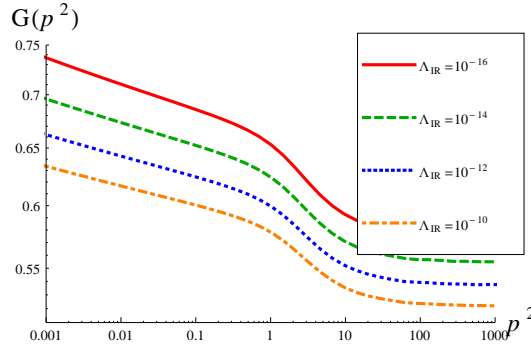


Figure 4. Ghost propagator dressing functions resulting from the decoupling type gluon propagator. The various curves correspond to different IR cutoffs.

Taylor argument [50] does not forbid a ghost-gluon vertex that is IR vanishing. Of course such a behavior is unlikely and unexpected, but one can construct a ghost-gluon vertex that allows a solution for the ghost equation also in this case. We also tried the opposite way, namely to solve the ghost-gluon vertex DSE using decoupling type ansätze for the propagators. However, in this case we could not find a solution. This further corroborates the non-existence of a decoupling type solution in two dimensions.

3.2 Influence of the mid-momentum regime on the ghost's UV behavior

Another important lesson from the ghost DSE alone concerns the influence of different momentum regions on each other. In four dimensions such an influence is subleading, mainly due to renormalization. In three dimensions, this is a weak quantitative effect [27]. For example, the UV behavior can be determined self-consistently. In two dimensions this is not the case. This can already be inferred from a purely perturbative investigation based on bare propagators which fails because of IR divergences which can only be remedied by taking into account a non-trivial behavior at momenta below the UV

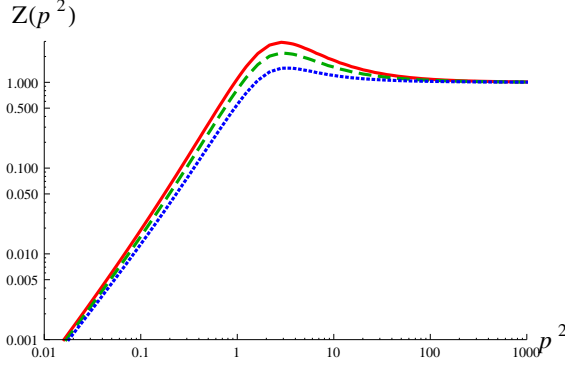


Figure 5. Input gluon propagator dressing functions given by Eq. (3.2) and $c_{gl} = 1, 0.7, 0.4$ (solid/red, dashed/green, dotted/blue).

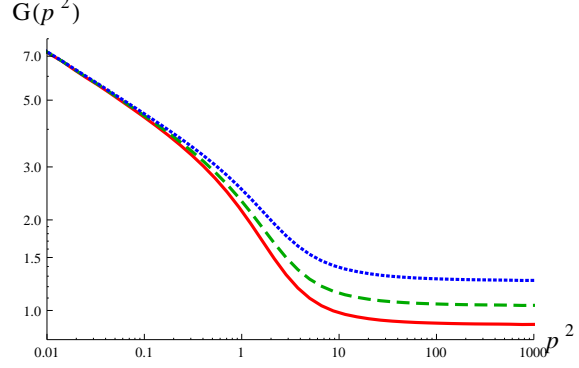


Figure 6. Ghost propagator dressing functions resulting from the gluon propagator ansätze given in Fig. 5 and a bare ghost-gluon vertex. Solid/red, dashed/green and dotted/blue lines correspond to $c_{gl} = 1, 0.7, 0.4$.

regime. We explicitly demonstrate the influence of the mid-momentum regime by studying the ghost DSE with the gluon dressing function given in Eq. (3.2) where we vary the parameter c_{gl} which modifies the height of the bump in the gluon dressing function. The ansätze for $c_{gl} = 0.4, 0.7, 1$ are shown in Fig. 5 and the resulting ghost dressing functions in Fig. 6. It is clearly visible that the height of the bump is correlated with the value of the ghost dressing function in the UV: The higher the bump the lower the ghost dressing becomes in the UV. This observation will be important later in Sec. 5 when we solve the DSEs of both propagators simultaneously. Note that the IR is not affected by the mid-momentum behavior.

4 The IR solutions revisited: Analytic considerations

4.1 The solution $\kappa = 0$

For the scaling type solution one can determine the qualitative behavior in the deep IR by calculating the IR exponents which can be done analytically [1, 3, 4]. Therefor one calculates the IR leading diagrams in the two-point DSEs, viz. the ghost loop in the gluon DSE and the loop of the ghost DSE, see Fig. 1, using the power law ansätze for the propagator dressing functions given in Eq. (2.5) together with the scaling relation Eq. (2.6):

$$Z^{IR}(p^2) = A \cdot (p^2)^{2\kappa+(d-4)/2}, \quad G^{IR}(p^2) = B \cdot (p^2)^{-\kappa}. \quad (4.1)$$

For the ghost-gluon vertex usually a bare vertex is employed but the same results for κ hold for all ghost-gluon vertices with a regular IR limit [4]. The IR value of the coupling, however, depends on the IR value of the vertex. The calculation of κ in d dimensions boils down to solving the following equation [3, 4]:

$$\frac{\sin(\pi\kappa)\Gamma(d/2-\kappa)\Gamma(\kappa)\Gamma(1+d/2+\kappa)}{2(d-1)\sin(\pi(d/2-2\kappa))\Gamma(d-2\kappa)\Gamma(2\kappa)\Gamma(1+\kappa)} = 1. \quad (4.2)$$

For two dimensions two solutions have been cited in Ref. [3]: $\kappa_1 = 0.2$, which is close to values extracted from lattice data [31, 46, 47], and $\kappa_2 = 0$. Note that the IR exponents of the propagators for

the second solution are $\delta_{gh} = 0$ and $\delta_{gl} = 1$ which are exactly the IR exponents of the decoupling type solutions. Hence the two-dimensional case is special in that a possible decoupling solution would also respect the scaling relation Eq. (2.6). We will now present further evidence against the decoupling type solution with κ_2 in addition to those presented in [34].

Let us scrutinize Eq. (4.2) for $d = 2$ and $\kappa = 0$. In Ref. [3] it was argued that for $d = 2 + \epsilon$ a solution $\kappa = 0 + \epsilon$ exists. This is illustrated in Fig. 7, where the left-hand side of Eq. (2.6) is plotted for $d = 1.9, 2, 2.1$. As d approaches 2 from either side, there are intersection points with unity which indeed approach $\kappa = 0$, such that there seems to be a solution also for $d = 2$. On the other hand, we can take the limit $d \rightarrow 2$ on the left-hand side analytically:

$$\frac{1 + \kappa}{2 - 4\kappa} = 1. \quad (4.3)$$

The only solution to this is $\kappa = 0.2$. The reason for this discrepancy is that $d = 2$ and $\kappa = 0$ corresponds to a multi-valued point and a wide range of possible values can be obtained. For example, we could approach the point by taking the limit $\epsilon \rightarrow 0$ and $d = 2 + 2\epsilon$ and $\kappa = \epsilon$. Then the left-hand side of Eq. (4.2) is one and $\kappa = 0$ is a solution. Note that in four dimensions the same arguments apply to the solution $\kappa = 1$. In three dimensions the mathematical existence of two solutions is unequivocal. Varying the number of dimensions continuously one sees that there are two branches of solutions [3, 27]. In four dimensions only one of those two solutions is found to be realized in numeric calculations [51], but in three dimensions solutions for both cases have been found [27]. Nonetheless, it may be hypothesized that only one branch is physical, namely the one on which $\kappa = 0.595353$ in four dimensions and $\kappa = 0.2$ in two dimensions lie. The presence of the second solution in three dimensions could be a truncation artifact, but this requires further investigations.

In summary, the infrared exponent κ_2 requires an additional prescription for how to define a two-dimensional solution in a particular limit $d \rightarrow 2$ suitably combined with $\kappa(d) \rightarrow 0$. This makes its existence scheme dependent and it seems at least questionable whether such a solution is realized. Since this solution coincides with the decoupling solution, such a type of solution seems, from this point of view, unlikely to exist in two dimensions.

4.2 Scaling solutions with $\kappa \neq 0.2$

Although lattice calculations seem to obtain a scaling type solution, it is not yet settled what the numerical value of κ is. First results corresponded to values of about 0.15 [31], but recent calculations on larger lattices seem to favor a value of 0.225 [47]. From functional equations, however, the value $\kappa = 0.2$ is well established [3, 4]. In the calculation of κ only the IR parts of the propagators and the ghost-gluon vertex enter. Hence modifications in the mid-momentum and UV regime are irrelevant as are any details of the three-gluon vertex as long as it is not more IR divergent than $(p^2)^{-3\kappa+(d-4)/2}$ [9, 28]. As far as the propagators are concerned only the combination $A B^2$ of the coefficients of the IR power laws from Eq. (2.5) enters and is calculated together with κ . The only quantity which has to be set by hand is the ghost-gluon vertex in the IR. A class of regular vertex dressings was investigated in Ref. [4], where it was shown that they all result in the same κ . Regularity means here that the ghost-gluon vertex dressing function has a unique IR limit when all momenta go to zero. Thus the only way to obtain a different value for κ is to allow non-regular vertex dressings, i. e., the IR limit depends on the angle between two momenta.

To implement such an angle dependence we employ the ansatz

$$D_{t,ad}^{A\bar{c}c}(k;p,q) = 1 + a (\cos \varphi)^2 \quad (4.4)$$

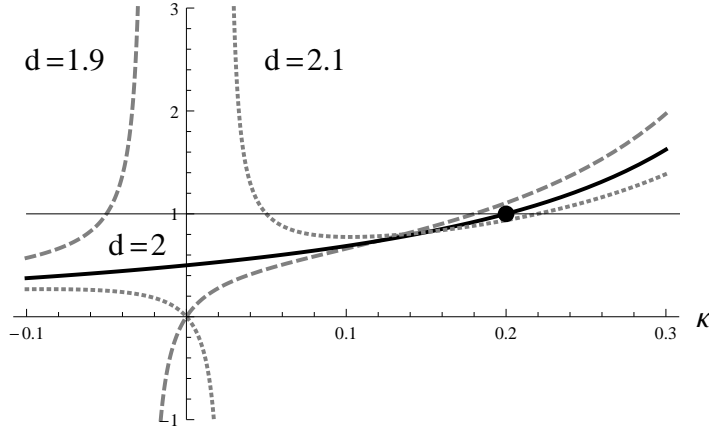


Figure 7. Left- and right hand sides of Eq. (4.2). The dashed, solid and dotted lines corresponds to $d = 1.9, 2, 2.1$, respectively. As d approaches 2, a solution seems to be $\kappa = 0$, but actually the point $d = 2, \kappa = 0$ is multi-valued. The blob at $\kappa = 0.2$ represents the standard solution.

for the transverse dressing function of the ghost-gluon vertex, where φ is the angle between the two ghost momenta:

$$\cos(\varphi) = \frac{p \cdot q}{|p||q|} = \frac{k^2 - p^2 - q^2}{2|p||q|}. \quad (4.5)$$

The angle is not well defined in the zero-momentum limit.

The ansatz (4.4) is motivated by the ghost-antighost symmetry in Landau gauge and corresponds to the first two terms in a Fourier series of more generally possible angle dependences [42]. The values for κ and the IR fixed-point value for the coupling, given by [2, 4, 28, 52]

$$\alpha(0) := \frac{g^2}{4\pi} A B^2, \quad (4.6)$$

can then be calculated using this ansatz. The results are depicted in Fig. 8. Figs. 9 and 10 show results for three and four dimensions, respectively, where the same arguments as in two dimensions apply.

Finally we want to make a comment on the dependence of κ on the employed projection of the gluon DSE. In principle any projection should yield the same value for κ , but since we have to use a truncated system of equations it actually does depend on the projection operator. For example, the Brown-Pennington projector leads to $\kappa = 0.224745$. However, any non-transverse projection leads to contributions from the longitudinal part of the ghost-gluon vertex. If we had the exact ghost-gluon vertex, this would be fine and we would get the same value of κ for all projections. Since we do not have the exact vertex, we will employ the transverse projection only. This disposes of the following ambiguity as shown in Ref. [4]: In general there exists a second gauge parameter which interpolates between the normal Faddeev-Popov action of linear covariant gauges and the ghost anti-ghost symmetric gauges. However, in the Landau gauge this parameter is irrelevant and thus any quantity depending on it is ambiguous. A transverse projector gets rid of all such terms. See also Ref. [53] for a short discussion of this issue.

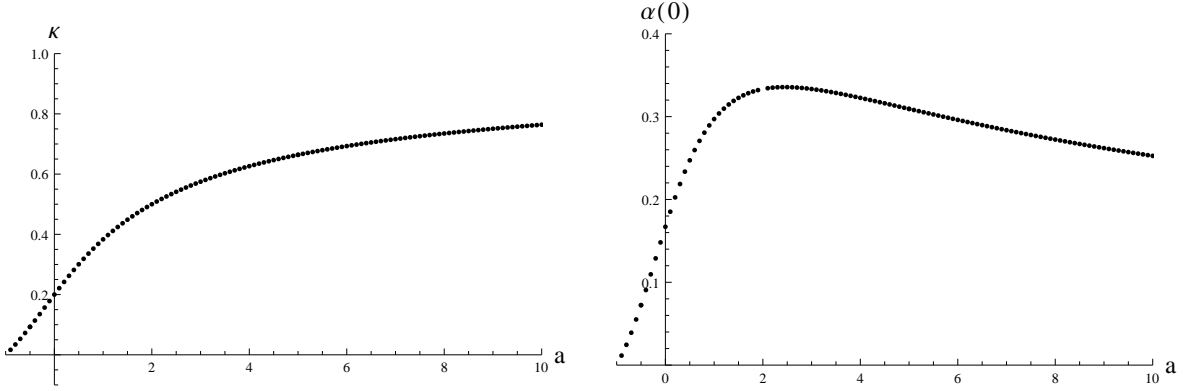


Figure 8. *Left:* κ for different values of a . *Right:* The corresponding values of $\alpha(0)$. Both plots are for two dimensions.

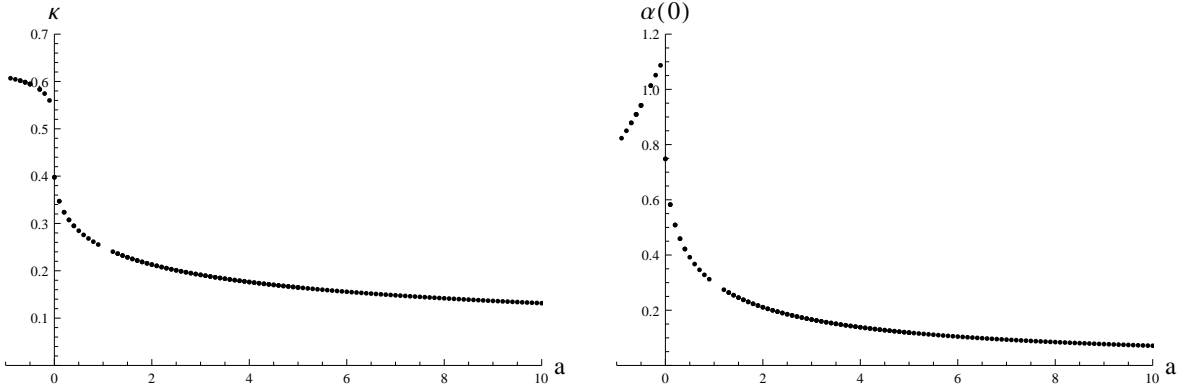


Figure 9. *Left:* κ for different values of a . *Right:* The corresponding values of $\alpha(0)$. Both plots are for three dimensions and only one solution branch is shown.

5 The coupled system of two-point DSEs

As a next step we solve the DSEs for the ghost and gluon two-point functions simultaneously. This system contains as a new quantity the three-gluon vertex for which we need an ansatz. An expression similar to the one used in four dimensions [51, 54] turns out to be insufficient, because the gluon loop will then dominate the ghost loop at intermediate momenta and the gluon dressing function turns negative. This was already observed in three dimensions [27] and motivated another construction for the three-gluon vertex. A similar one for two dimensions is

$$D_{ans}^{A^3}(p, q, r) = \left(\frac{(G(p^2)G(q^2)G(k^2))^{-2-1/\kappa}}{Z(p^2)Z(q^2)Z(k^2)} \right)^\alpha. \quad (5.1)$$

This expression becomes 1 for large momenta and is suppressed for low ones. The exponent α controls the strength of the suppression. In order to find a solution it must not be too small. However, it is known that the three-gluon vertex is not IR suppressed but actually IR enhanced in two [28, 31], three [18, 28] and four dimensions [9, 18]. In two dimensions, an approximate agreement between

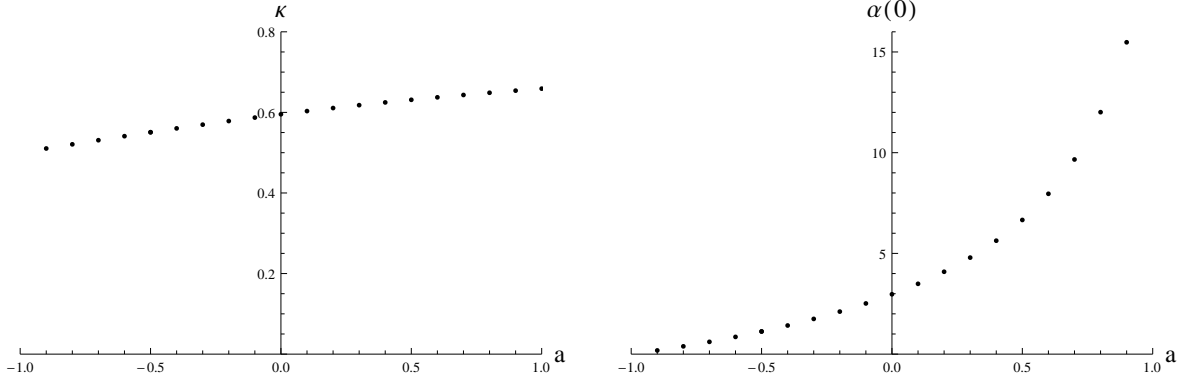


Figure 10. *Left:* κ for different values of a . *Right:* The corresponding values of $\alpha(0)$. For $a \gtrsim 1.3$ the coupling becomes negative and is not shown. Both plots are for four dimensions.

the prediction from functional methods [28] and the lattice results [31] is found, while in higher dimensions the lattice results [18] do not yet penetrate very far into the infrared. Furthermore, lattice calculations showed that the three-gluon vertex changes its sign at intermediate momenta [18, 31]. For two dimensions we show in Appendix B that the DSE of the three-gluon vertex reproduces this zero crossing. Based on this behavior we adopt the following ansatz for the dressing function of the three-gluon vertex:

$$D_{mod}^{A^3}(p, q, r) = \frac{p^2 + q^2 + r^2}{p^2 + q^2 + r^2 + h_{IM}\Lambda^2} + h_{IR}(p^2 + q^2 + r^2)^{-3\kappa-1}. \quad (5.2)$$

The first term ensures the correct UV behavior and the second term implements the IR divergence [28]. Note that the parameter h_{IR} has to be negative in order to reproduce the zero crossing. h_{IR} can be obtained by a fit to lattice data. However, in order to obtain a solution we have to choose a much higher absolute value in order to compensate for dropping the two-loop diagrams in our truncation.

As in four dimensions the gluon DSE contains spurious divergences. They are the remnants of the quadratic divergences in four dimensions which arise due to the use of a UV cutoff as regulator and thus appear already at the perturbative level [26]. One possibility to handle these logarithmic divergences is to modify the integrand of the gluon loop such that the logarithmic divergences cancel [51, 54]. Another possibility is to employ a counter term, akin to the minimal subtraction scheme from perturbation theory [26, 27]. The divergences appear in the gluon two-point DSE in the following form:

$$\frac{1}{Z(p^2)} = 1 + \Sigma(p^2) = 1 + \frac{g^2}{p^2}\Sigma'(p^2) + c g^2 \frac{\ln \Lambda^2}{p^2}, \quad (5.3)$$

where $\Sigma(p^2)$ is logarithmically divergent and $\Sigma'(p^2)$ is finite. Subtracting from this the self-energy at the momentum s times s^2/p^2 yields

$$\frac{1}{Z(p^2)} - \frac{1}{Z(s^2)} \frac{s^2}{p^2} = \Sigma(p^2) - \Sigma(s^2) \frac{s^2}{p^2} = \frac{g^2}{p^2}\Sigma'(p^2) - \frac{g^2}{p^2}\Sigma'(s^2), \quad (5.4)$$

i. e., the logarithmic divergence is gone. Since the logarithmic divergences only reside in the part proportional to $p_\mu p_\nu$, it is advantageous to use the longitudinally projected self-energy for the subtraction term since this interferes least with the physical part. The two methods for subtracting the logarithmic divergences are compared in Fig. 11.

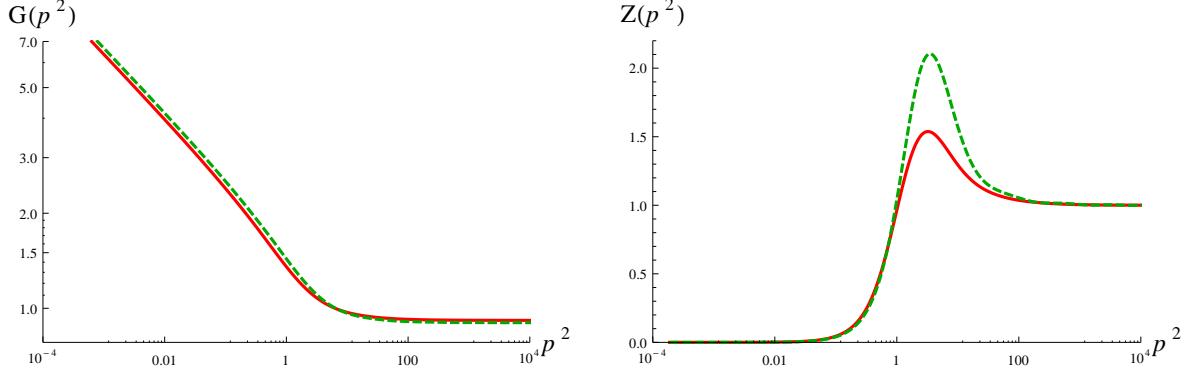


Figure 11. Ghost (*left*) and gluon (*right*) dressings obtained with a bare ghost-gluon vertex and the three-gluon vertex of Eq. (5.1) with $\alpha = 0.15$. The red/solid lines result from subtracting the logarithmic divergences in the gluon loop kernel, while green/dashed lines stem from using the subtraction Eq. (5.4).

5.1 Bare ghost-gluon vertex

The use of a bare ghost-gluon vertex is standard in three and four dimensions, see, for example, [3, 4, 16, 17, 27, 30, 55]. The small deviations from the tree-level observed by lattice calculations [18, 56–58] do not affect the IR or UV behavior and influence only the mid-momentum regime. A semi-perturbative DSE analysis of the vertex [59] yielded qualitatively similar results as from lattice calculations. Therefore we start our investigations with a bare ghost-gluon vertex. The resulting propagator dressings are shown in Fig. 12. It turns out that the ghost dressing function does not approach one in the UV. However, since the dimension of the coupling constant is that of momentum we know from dimensional arguments that it should behave for large momenta as

$$G(p^2) \xrightarrow{p^2 \rightarrow \infty} \frac{1}{1 + c g^2/p^2} \quad (5.5)$$

with c a constant. Also lattice calculations [31] confirm that the ghost should be close to one in the UV.

Based on this deviation of the ghost dressing function we conclude that the employed truncation is insufficient. The reason for this is a rather intricate relation in the ghost DSE. Its unsubtracted form has the structure

$$\frac{1}{G(p^2)} = 1 + \Sigma(p^2).$$

For large momenta, asymptotic freedom requires that $\Sigma(p^2)$ vanishes, and thus the ghost dressing function approaches necessarily one. At low momenta, $\Sigma(p^2)$ will behave in the scaling case as $a + A(p^2)^\kappa + \mathcal{O}((p^2)^\delta)$ with some constant a and $\delta > \kappa$. Only when $a = -1$, the scaling solution can be a solution to the equation. This requires that Σ must provide a large enough integrated strength. Due to the integral measure, the far infrared does not contribute to this, and due to asymptotic freedom neither does the ultraviolet. Thus, $a = -1$ must be provided by the mid-momentum behavior. This can be generated by two ingredients. One is the mid-momentum enhancement of the gluon dressing, its maximum. The other is due to an enhancement of the ghost-gluon vertex. Here, we find that for a dressing function of the gluon, which is not exceeding the lattice results significantly, $a = -1$ cannot

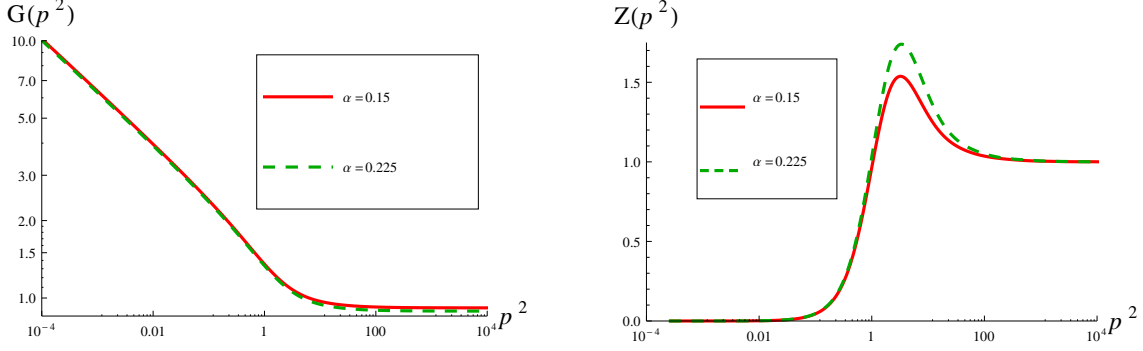


Figure 12. Propagator dressing functions using a bare ghost-gluon vertex and the three-gluon vertex ansatz given in Eq. (5.1) with $\alpha = 0.15, 0.225$. *Left:* Ghost dressing function. In the UV the values are 0.92 and 0.89. *Right:* Gluon dressing function.

be achieved with a bare ghost-gluon vertex. This is different from three dimensions, where this is possible [27]. In four dimensions, this problem is alleviated, as the one in the ghost equation can be modified by a wave-function renormalization to any desired value [21], and the problem thus does not exist.

5.2 Ghost-gluon vertex model

Having identified the source of the problem of the UV behavior of the ghost dressing function we will now attempt to improve the results by using more elaborate ansätze for the three-point functions motivated by lattice results. In the following we will only use the transversely projected gluon DSE, so we only need to model the dressing function $D_t^{A\bar{c}c}$ of the ghost gluon vertex which we take as

$$D_{t,mod}^{A\bar{c}c}(r, p, q) = 1 + \frac{1}{\Lambda^2 + p^2 + q^2 + r^2} \left(f_{IR} + f_{IM} \frac{\Lambda^2(p^2 + q^2)}{\Lambda^4 + p^4 + q^4} \right). \quad (5.6)$$

The new term proportional to f_{IM} adds a bump in the mid-momentum regime as seen in lattice calculations [31]. This bump occurs also in three and four dimensions, see refs. [18, 56, 57], where it was also reproduced by a semi-perturbative DSE calculation [59]. The parameter f_{IR} sets the IR value of the dressing and Λ is a scale parameter. This form of the vertex leaves the value of κ unchanged as discussed in Sec. 4.2, but not the IR value of the coupling, which scales with $1/(1 + f_{IR}/\Lambda^2)$.

For the three-gluon vertex we will continue to consider only one dressing given by Eq. (5.2), because adding dressings will not change anything qualitatively and one dressing is sufficient for our purposes. Fixing the parameters of the ghost-gluon vertex it is indeed possible to tune the three-gluon vertex parameters such that the ghost dressing function becomes one in the UV. A possible choice of parameter values is given in Table 1 and the resulting dressing functions are plotted in Fig. 13.

A remarkable feature of these and the following results is that they cure the infrared singularities of perturbation theory. This is not so surprising when considering loops including gluons due to the infrared suppression of their propagator. For the ghost-loop in the gluon equation, however, this is naively unexpected, given that the ghost propagator is infrared more divergent as in perturbation theory. The explanation are intricate cancellations in the angular loop integral due to the non-trivial momentum dependencies of the dressing functions, emphasizing the delicate balancing in scaling type solutions.

Parameter	Value
Λ	1
f_{IR}	2.14189
f_{IM}	0.6
h_{IR}	-71.5
h_{IM}	9.88

Table 1. Values employed for the parameters of the ghost-gluon and three-gluon vertex ansätze given in eqs. (5.6) and (5.2), respectively.

Parameter	Value
Λ	1
h_{IR}	-31.57
h_{IM}	9.88

Table 2. Values employed for the parameters of the three-gluon vertex ansatz given in Eq. (5.2) when including the ghost-gluon vertex dynamically.

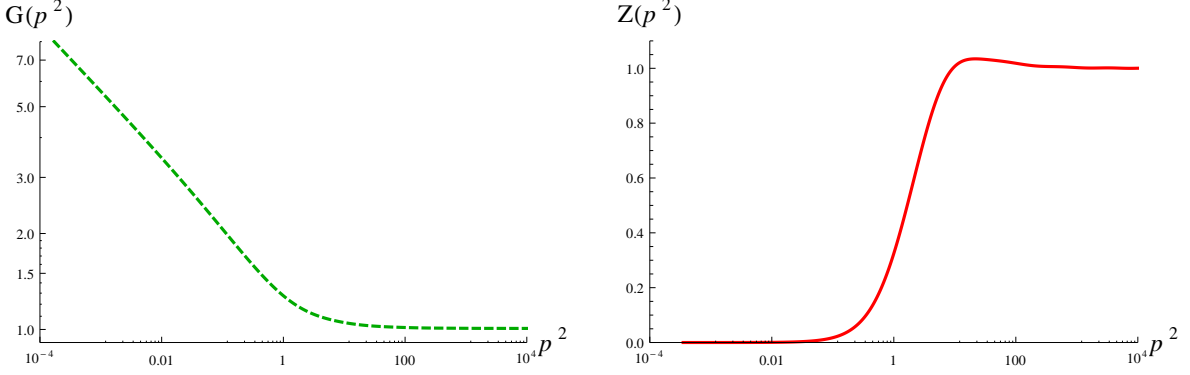


Figure 13. Ghost (*left*) and gluon (*right*) dressings obtained with the models given in eqs. (5.6) and (5.2) using the values of Table 1 for the parameters.

6 Including the ghost-gluon vertex dynamically

Knowing how important the three-point functions are for the correct UV behavior of the ghost propagator we will now include the ghost-gluon vertex dynamically into our calculations. Working in two dimensions is thereby advantageous because we only have to calculate two-dimensional integrals, whereas in three and four dimensions the integrals are three-dimensional. Furthermore, in contrast to four dimensions, the UV behavior is trivial. This calculation is therefore also an exploratory study for future calculations in four dimensions which extend the currently employed truncation schemes beyond the propagators.

We will again use the transversely projected gluon DSE so that only one dressing function of the ghost-gluon vertex is relevant. Three-point functions depend on three variables for which we choose the squares of the two ghost momenta and the angle φ between them. The vertex is calculated for a grid in these variables. For intermediate points we use linear interpolation. If any momentum is outside the grid we use the value of the dressing at its boundary. Considering the increased complexity of the ghost-gluon vertex DSE it was advantageous to derive the kernels with the program *DoFun* [44, 48]. For solving the DSEs the framework provided by *CrasyDSE* [60] was used.

The ghost-gluon vertex has two distinct DSEs, which differ by the field that is attached to the bare vertex. We take the DSE where this is the gluon field. Although this DSE seems more complicated than the other one, since it has more terms, it turns out that in our truncation scheme it is simpler. The full DSE is shown in Fig. 14. The first step of our truncation consists in discarding all diagrams

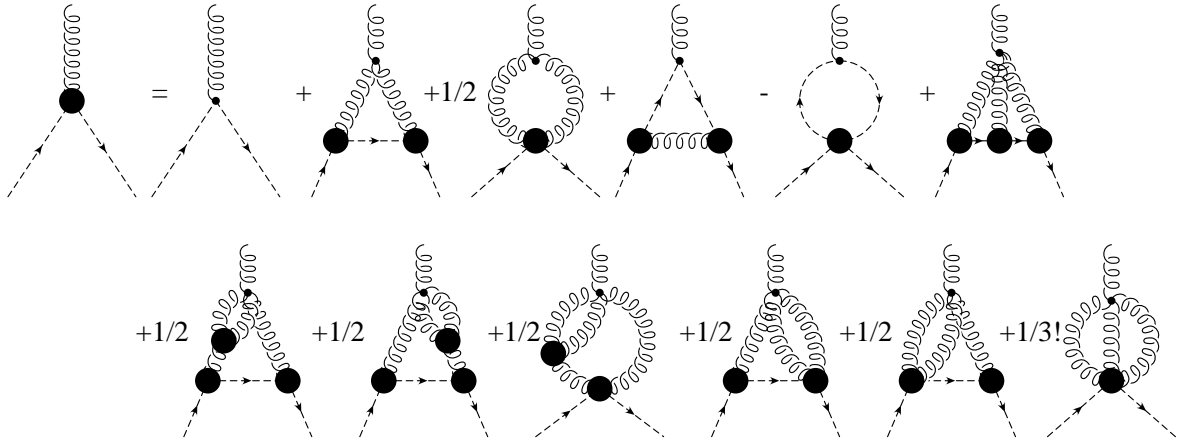


Figure 14. The ghost-gluon vertex DSE. All internal propagators are dressed. Thick blobs denote dressed vertices. Wiggly lines are gluons, dashed ones ghosts. The employed truncation consists of the first, the second and the fourth diagrams.

containing a bare four-gluon vertex, i. e., all two-loop diagrams. Of the remaining diagrams the ones with a bare ghost-gluon vertex dominate in the IR [28]. Furthermore, we keep only the diagrams of leading order in the UV, so we discard the third and fifth diagrams on the right-hand side. Although the latter is at leading order in the IR it does not represent one of the main contributions there, because when we insert the DSE of the irreducible quartic ghost vertex, we see that the IR leading contribution is a two-loop diagram and should give only a minor correction to the IR behavior of the ghost-gluon vertex. As attested by our calculations below already the fourth diagram yields only small corrections to the bare vertex.

The resulting dressings of the propagators and the ghost-gluon vertex are shown in Figs. 15 and 16, respectively. For comparison the plots of the propagator dressings also contain results presented in the previous sections. The differences originating in the mid-momentum regime can clearly be seen. Most notably the maximum of the gluon dressing function is driven to even larger momenta and becomes more shallow. In the ghost-gluon vertex dressing also a bump in the mid-momentum regime is seen. However, it can be uniquely traced back to the second diagram on the right-hand of its DSE in Fig. 14. We also tried the second version of the ghost-gluon vertex DSE, but we did not obtain a solution. The reason is that in this DSE the dressed instead of the bare three-gluon vertex appears and introduces an instability in the system of equations. This again illustrates the delicate balancing in the mid-momentum regime in two dimensions.

Comparing the presented results with lattice data, we see that they do not agree as much as expected from three and four dimensions. Most likely these discrepancies could be compensated by the two-loop diagrams in the gluon equation and other neglected diagrams in the ghost-gluon vertex DSE. However, currently the inclusion of two-loop diagrams in DSEs has not been explored thoroughly enough to implement them here straightforwardly, but see, for example, [61, 62]. The main reason that they have been neglected in the literature so far is that they yield only subleading contributions both in the IR and the UV for the Landau gauge in three and four dimensions [9, 28]. Furthermore, their increased complexity requires to extend currently employed methods [62]. Thus, though in two dimensions the qualitative properties of the solution of the DSEs is more simple and unambiguous,

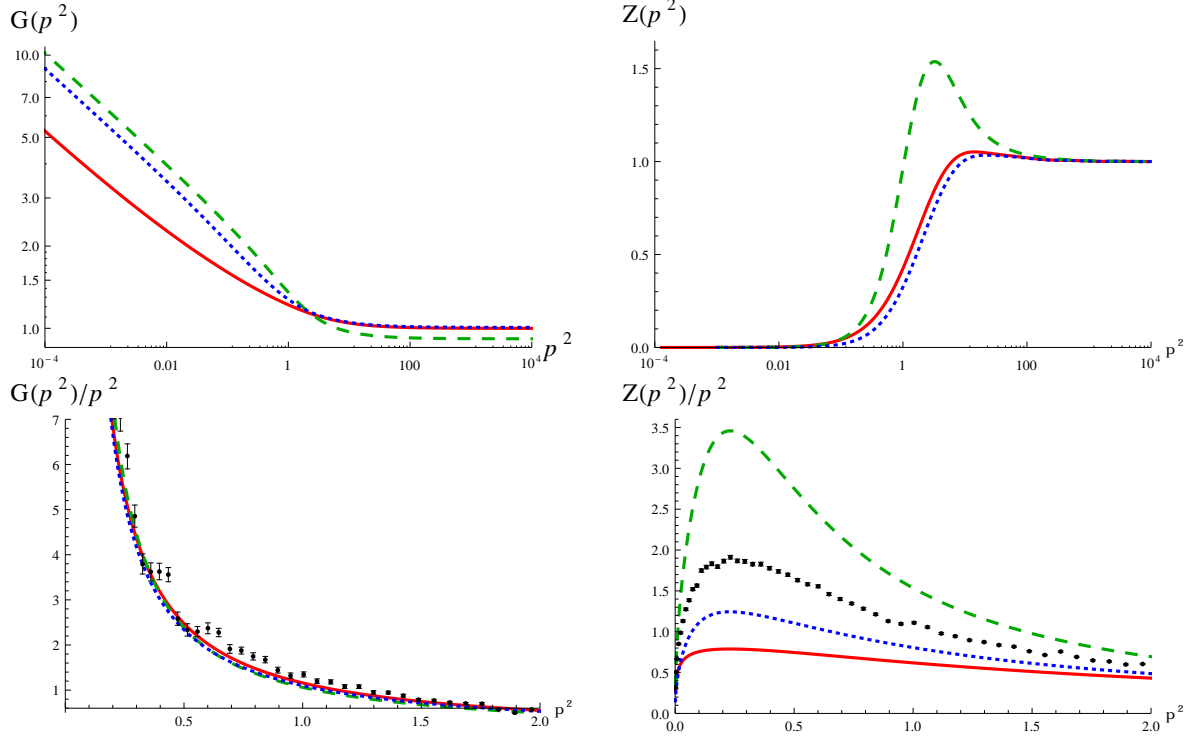


Figure 15. Ghost (*left*) and gluon (*right*) dressings obtained when including the ghost-gluon vertex dynamically (red/solid lines) and using the three-gluon vertex ansatz from Eq. (5.2) with parameters given in Table 2 compared to the results when using a bare ghost-gluon vertex (green/dashed lines) or the model from Eq. (5.6) (blue/short-dashed line) with parameters given in Table 1. *Bottom:* Comparison of the propagators with lattice data (black points) from [26]. In the plot of the ghost propagators the continuum results are nearly indistinguishable. Scale set by matching the positions of the maxima in the gluon propagators. Note that this rescaling is responsible for the interchange of the blue/short-dashed line with the red/solid line.

the quantitative features are not described as satisfactorily as in three and four dimensions. In four dimensions this difference is likely due to the possibility of renormalization, which permits to shift various effects to different momentum scales. In three dimensions, where one also finds quantitatively acceptable descriptions of the mid-momentum regime, it is probably due to the increased contribution from the momentum integral measure, which permits rather small differences at larger momenta to have already a significant impact.

7 Conclusions

Summarizing, we have provided the first full solution of the two-dimensional DSEs, including the equation for the propagators *and* the ghost-gluon vertex. The inclusion of the latter was necessary, as we found that the mixing of different momentum regimes in superrenormalizable theories invalidates the simple truncations used in the four-dimensional, renormalizable case. The reasons for this can be understood and lie in the intricate cancellations necessary for a scaling type solution, which we find, in accordance with [34], to be the only viable type of solution in two dimensions. That a similar

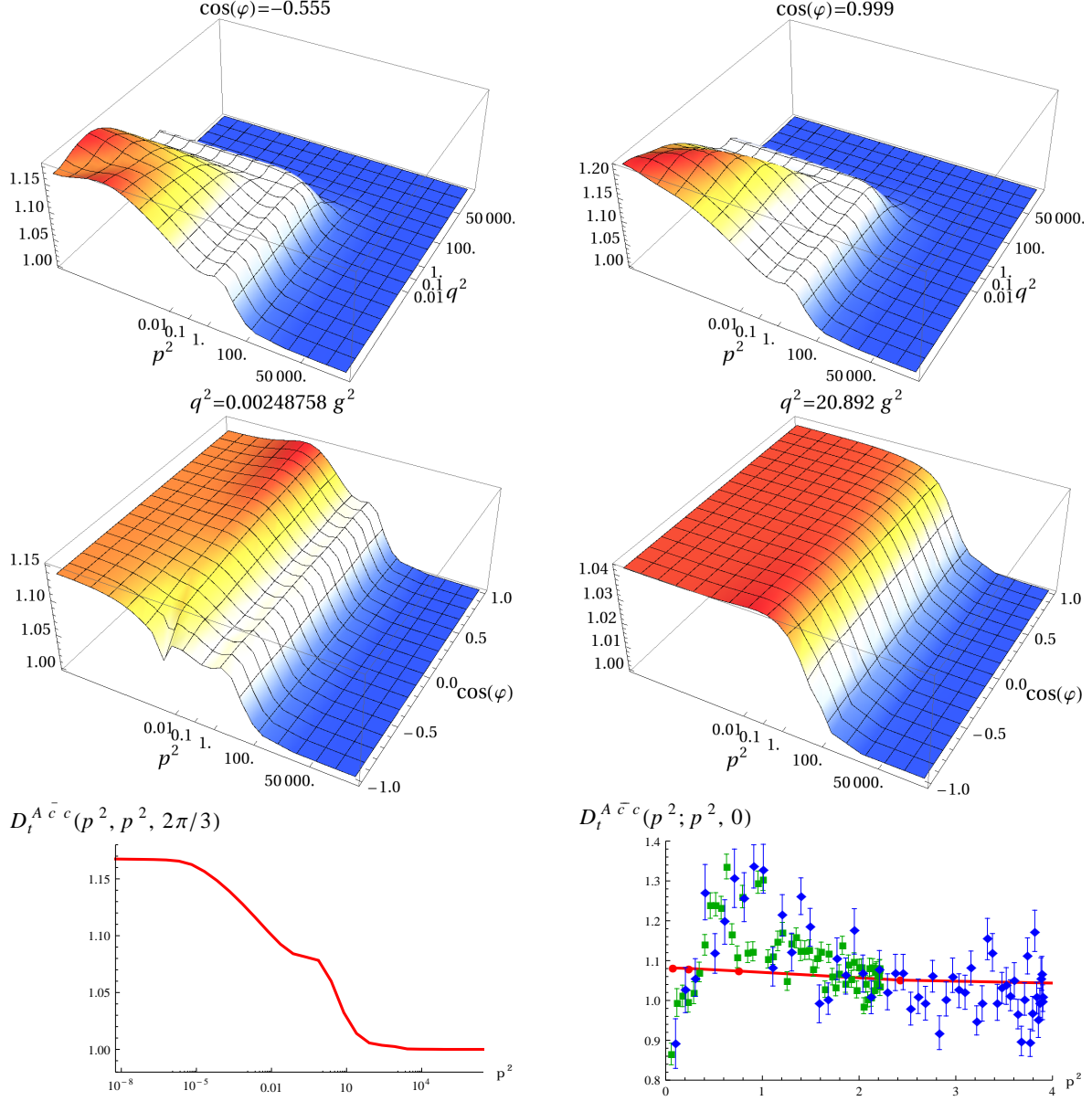


Figure 16. Dressing of the ghost-gluon vertex for various momentum configurations obtained from the coupled system of propagators and the vertex itself. For the three-gluon vertex the ansatz of Eq. (5.2) with the parameters of Table 2 was used. *Top:* Fixed angle as indicated at the top of each plot. *Middle:* Fixed momentum q^2 as indicated at the top of each plot. Note the different scales on the z -axes. *Bottom:* On the left the symmetric configuration is shown. Since this configuration cannot be realized on the lattice, no comparison with lattice data is possible. The bump stems from the non-Abelian diagram. On the right the gluon momentum and one ghost momentum are orthogonal. The red/solid line is the result from the DSE calculation and green squares are for $\beta = 10/L = 21 fm^{-1}$ and blue diamonds for $\beta = 22.5/L = 12 fm^{-1}$. Lattice data from Ref. [31].

situation did not arise in this severeness in earlier studies in three dimensions [27] must be attributed with hindsight to quantitative effects.

As a consequence, the results here have not yet reached a maturity as in higher dimensions when it comes to quantitatively reproducing lattice results. This will require much more sophisticated truncation schemes, which will likely require the inclusion of two-loop terms. In DSEs, this is a formidable endeavor, and thus a renormalization group approach, with its intrinsic one-loop structure, may be more adequate. Nonetheless, we reproduced all qualitative features and provided an understanding of the underlying mechanisms.

Acknowledgments

M.Q.H. was supported by the Alexander von Humboldt foundation, A.M. by the DFG under grant number MA 3935/5-1, and L.vS. by the Helmholtz International Center for FAIR within the LOEWE program of the State of Hesse, the Helmholtz Association Grant VH-NG-332, and the European Commission, FP7-PEOPLE-2009-RG No. 249203. Plots of DSEs were created with *FeynDiagram* and *JaxoDraw* [63].

A Kernels

The kernel K_G of the ghost DSE given in Eq. (2.7) is

$$K_G(p, q) = \frac{(x^2 + (y - z)^2 - 2x(y + z))}{4xy^2z} \quad (\text{A.1})$$

with $x = p^2$, $y = q^2$ and $z = (p + q)^2$. The two kernels K_Z^{gh} and K_Z^{gl} of the gluon DSE Eq. (2.8) read

$$\begin{aligned} K_Z^{gh}(p, q) &= -\frac{(x^2 + (y - z)^2 - 2x(y + z))}{4x^2yz}, \\ K_Z^{gl}(p, q) &= \frac{x^4 - 8xyz(y + z) + x^2(-2y^2 - 8yz - 2z^2) + (y - z)^2(y^2 + 2yz + z^2)}{8x^2y^2z^2}. \end{aligned} \quad (\text{A.2})$$

In order to get rid of the logarithmic divergences in the gluon DSE without using counter terms, the following expression is added to the kernel of the gluon loop K_Z^{gl} :

$$K_Z^{gl,sub}(p, q) = \frac{1}{2xy}. \quad (\text{A.3})$$

The kernels for the ghost-gluon vertex are too lengthy to be reproduced here. They were generated automatically using the programs *DoFun* [44, 48] and *CrasyDSE* [60] using the ansätze for the vertices as described in the main text.

B Three-gluon vertex

For solving the coupled system of propagators and ghost-gluon vertex in Sec. 6 we employed a lattice inspired ansatz for the three-gluon vertex. Here we calculate the three-gluon vertex using the results obtained there for illustration and comparison. A combined calculation of propagators and both three-point functions did not yield a stable iteration which is again due to the effect truncations have on the mid-momentum regime. Nevertheless it is interesting to see that the lattice results can be

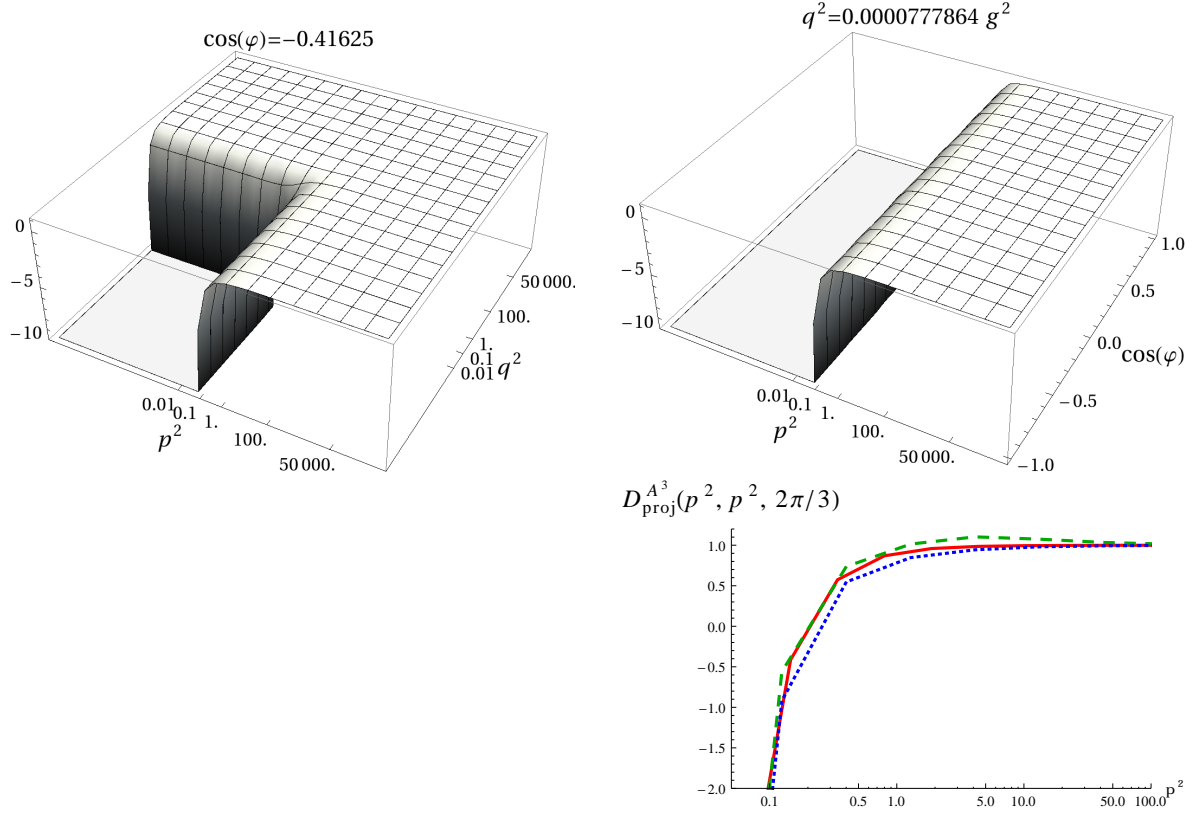


Figure 18. Dressing of the three-gluon vertex, see Eq. (B.1). Only the beginning of the IR divergence is shown by cutting all data below -10 . *Top left:* Angle fixed at $\arccos(-0.41625)$. *Top right:* One momentum is fixed at $\sqrt{0.00007786} g$. *Bottom right:* Symmetric configuration. The solid/red line is with the ghost triangle only, the dashed/green one with both triangles and the dotted/blue line with all five diagrams.

the three-gluon vertex onto itself. As expected, the details of the mid-momentum regime depend on the employed truncation, whereas the IR and UV regime are unaffected.

References

- [1] L. von Smekal, A. Hauck, and R. Alkofer, *Ann. Phys.* **267** (1998) 1, [arXiv:hep-ph/9707327](#).
- [2] L. von Smekal, R. Alkofer, and A. Hauck, *Phys. Rev. Lett.* **79** (1997) 3591–3594, [arXiv:hep-ph/9705242](#).
- [3] D. Zwanziger, *Phys. Rev.* **D65** (2002) 094039, [arXiv:hep-th/0109224](#).
- [4] C. Lerche and L. von Smekal, *Phys. Rev.* **D65** (2002) 125006, [arXiv:hep-ph/0202194](#).
- [5] D. Zwanziger, *Phys. Rev.* **D67** (2003) 105001, [hep-th/0206053](#).
- [6] C. S. Fischer and R. Alkofer, *Phys. Lett.* **B536** (2002) 177–184, [arXiv:hep-ph/0202202](#).
- [7] J. M. Pawłowski, D. F. Litim, S. Nedelko, and L. von Smekal, *Phys. Rev. Lett.* **93** (2004) 152002, [arXiv:hep-th/0312324](#).

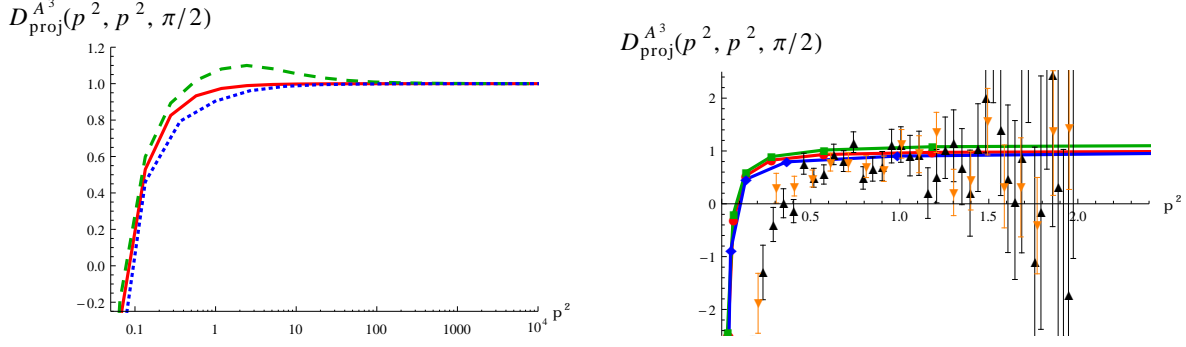


Figure 19. Three-gluon vertex dressing for two orthogonal momenta. *Left:* The red/solid curve results from using the ghost triangle alone, the green/dashed curve from ghost and gluon triangles and the blue/dotted curve from all five diagrams. The data is cut at the bottom to highlight the mid-momentum behavior. *Right:* Comparison with lattice data. The red/solid, green/dashed and blue/dotted curves are from the DSE calculations as on the left-hand side, the dots are from lattice calculations [31]. Black up-triangles are for $\beta = 10/L = 21 fm^{-1}$ and orange down-triangles for $\beta = 22.5/L = 12 fm^{-1}$. The data is cut at the bottom and for the lattice data also in the UV, since the fluctuations are very large there.

- [8] D. Zwanziger, *Phys. Rev.* **D69** (2004) 016002, [arXiv:hep-ph/0303028](#).
- [9] R. Alkofer, C. S. Fischer, and F. J. Llanes-Estrada, *Phys. Lett.* **B611** (2005) 279–288, [arXiv:hep-th/0412330](#).
- [10] P. Silva and O. Oliveira, *Nucl. Phys.* **B690** (2004) 177–198, [arXiv:hep-lat/0403026](#) [[hep-lat](#)].
- [11] I. L. Bogolubsky, E. M. Ilgenfritz, M. Müller-Preussker, and A. Sternbeck, *PoS LAT2007* (2007) 290, [arXiv:0710.1968](#) [[hep-lat](#)].
- [12] O. Oliveira and P. J. Silva, *Eur. Phys. J.* **C62** (2009) 525–534, [arXiv:0705.0964](#) [[hep-lat](#)].
- [13] A. Cucchieri and T. Mendes, *PoS LAT2007* (2007) 297, [arXiv:0710.0412](#) [[hep-lat](#)].
- [14] D. Dudal, S. P. Sorella, N. Vandersickel, and H. Verschelde, *Phys. Rev.* **D77** (2008) 071501, [arXiv:0711.4496](#) [[hep-th](#)].
- [15] D. Dudal, J. A. Gracey, S. P. Sorella, N. Vandersickel, and H. Verschelde, *Phys. Rev.* **D78** (2008) 065047, [arXiv:0806.4348](#) [[hep-th](#)].
- [16] P. Boucaud *et al.*, *JHEP* **06** (2008) 012, [arXiv:0801.2721](#) [[hep-ph](#)].
- [17] A. Aguilar, D. Binosi, and J. Papavassiliou, *Phys. Rev.* **D78** (2008) 025010, [arXiv:0802.1870](#) [[hep-ph](#)].
- [18] A. Cucchieri, A. Maas, and T. Mendes, *Phys. Rev.* **D77** (2008) 094510, [arXiv:0803.1798](#) [[hep-lat](#)].
- [19] R. Alkofer, M. Q. Huber, and K. Schwenzer, *Eur. Phys. J.* **C62** (2009) 761–781, [arXiv:0812.4045](#) [[hep-ph](#)].
- [20] R. Alkofer, M. Q. Huber, and K. Schwenzer, *Phys. Rev.* **D81** (2010) 105010, [arXiv:0801.2762](#) [[hep-th](#)].
- [21] C. S. Fischer, A. Maas, and J. M. Pawłowski, *Annals Phys.* **324** (2009) 2408–2437, [arXiv:0810.1987](#) [[hep-ph](#)].
- [22] L. von Smekal, [arXiv:0812.0654](#) [[hep-th](#)], Plenary talk at 13th International Conference on Selected Problems of Modern Theoretical Physics (SPMTP 08), Dubna, Russia, 23-27 Jun 2008.

- [23] C. S. Fischer and J. M. Pawłowski, *Phys. Rev.* **D80** (2009) 025023, [arXiv:0903.2193 \[hep-th\]](#).
- [24] M. Q. Huber, R. Alkofer, and S. P. Sorella, *Phys. Rev.* **D81** (2010) 065003, [arXiv:0910.5604 \[hep-th\]](#).
- [25] D. Zwanziger, *Phys. Rev.* **D81** (2010) 125027, [arXiv:1003.1080 \[hep-ph\]](#).
- [26] A. Maas, [arXiv:1106.3942 \[hep-ph\]](#).
- [27] A. Maas, J. Wambach, B. Grüter, and R. Alkofer, *Eur. Phys. J.* **C37** (2004) 335–357, [hep-ph/0408074](#).
- [28] M. Q. Huber, R. Alkofer, C. S. Fischer, and K. Schwenzer, *Phys. Lett.* **B659** (2008) 434–440, [arXiv:0705.3809 \[hep-ph\]](#).
- [29] D. Dudal, J. A. Gracey, S. P. Sorella, N. Vandersickel, and H. Verschelde, *Phys. Rev.* **D78** (2008) 125012, [arXiv:0808.0893 \[hep-th\]](#).
- [30] A. C. Aguilar, D. Binosi, and J. Papavassiliou, *Phys. Rev.* **D81** (2010) 125025, [arXiv:1004.2011 \[hep-ph\]](#), Decoupling 3d.
- [31] A. Maas, *Phys. Rev.* **D75** (2007) 116004, [arXiv:0704.0722 \[hep-lat\]](#).
- [32] D. Dudal, S. P. Sorella, N. Vandersickel, and H. Verschelde, *Phys. Lett.* **B680** (2009) 377–383, [arXiv:0808.3379 \[hep-th\]](#).
- [33] A. Cucchieri and T. Mendes, *AIP Conf.Proc.* **1343** (2011) 185–187, [arXiv:1101.4779 \[hep-lat\]](#).
- [34] A. Cucchieri, D. Dudal, and N. Vandersickel, *Phys.Rev.* **D85** (2012) 085025, [arXiv:1202.1912 \[hep-th\]](#).
- [35] J. M. Pawłowski, *AIP Conf.Proc.* **1343** (2011) 75–80, [arXiv:1012.5075 \[hep-ph\]](#).
- [36] J. Berges, N. Tetradis, and C. Wetterich, *Phys. Rept.* **363** (2002) 223–386, [arXiv:hep-ph/0005122](#).
- [37] J. M. Pawłowski, *Annals Phys.* **322** (2007) 2831–2915, [arXiv:hep-th/0512261](#).
- [38] H. Gies, [arXiv:hep-ph/0611146](#), Presented at ECT* School on Renormalization Group and Effective Field Theory Approaches to Many-Body Systems, Trento, Italy, 27 Feb - 10 Mar 2006.
- [39] O. J. Rosten, *Phys.Rept.* **511** (2012) 177–272, [arXiv:1003.1366 \[hep-th\]](#).
- [40] C. D. Roberts and A. G. Williams, *Prog. Part. Nucl. Phys.* **33** (1994) 477–575, [hep-ph/9403224](#).
- [41] C. D. Roberts and S. M. Schmidt, *Prog. Part. Nucl. Phys.* **45** (2000) S1–S103, [arXiv:nucl-th/0005064](#).
- [42] R. Alkofer and L. von Smekal, *Phys. Rept.* **353** (2001) 281, [arXiv:hep-ph/0007355](#).
- [43] C. S. Fischer, *J. Phys.* **G32** (2006) R253–R291, [arXiv:hep-ph/0605173](#).
- [44] R. Alkofer, M. Q. Huber, and K. Schwenzer, *Comput. Phys. Commun.* **180** (2009) 965–976, [arXiv:0808.2939 \[hep-th\]](#).
- [45] D. Binosi and J. Papavassiliou, *Phys. Rept.* **479** (2009) 1–152, [arXiv:0909.2536 \[hep-ph\]](#).
- [46] A. Maas, J. M. Pawłowski, D. Spielmann, A. Sternbeck, and L. von Smekal, *Eur.Phys.J.* **C68** (2010) 183–195, [arXiv:0912.4203 \[hep-lat\]](#).
- [47] A. Cucchieri, D. Dudal, T. Mendes, and N. Vandersickel, *Phys.Rev.* **D85** (2012) 094513, [arXiv:1111.2327 \[hep-lat\]](#).
- [48] M. Q. Huber and J. Braun, *Comput.Phys.Commun.* **183** (2012) 1290–1320, [arXiv:1102.5307 \[hep-th\]](#).
- [49] S. Wolfram, *The Mathematica Book*. Wolfram Media and Cambridge University Press, 2004.
- [50] J. C. Taylor, *Nucl. Phys.* **B33** (1971) 436–444.
- [51] C. S. Fischer, R. Alkofer, and H. Reinhardt, *Phys. Rev.* **D65** (2002) 094008, [arXiv:hep-ph/0202195](#).

- [52] L. von Smekal, K. Maltman, and A. Sternbeck, *Phys.Lett.* **B681** (2009) 336–342, [arXiv:0903.1696 \[hep-ph\]](#).
- [53] C. S. Fischer and L. von Smekal, *AIP Conf.Proc.* **1343** (2011) 247–249, [arXiv:1011.6482 \[hep-ph\]](#).
- [54] C. S. Fischer, [arXiv:hep-ph/0304233 \[hep-ph\]](#), Ph.D. thesis, Eberhard-Karls-Universität zu Tübingen (2003).
- [55] C. S. Fischer and R. Alkofer, *Phys. Rev.* **D67** (2003) 094020, [arXiv:hep-ph/0301094](#).
- [56] A. Cucchieri, T. Mendes, and A. Mihara, *JHEP* **12** (2004) 012, [hep-lat/0408034](#).
- [57] A. Cucchieri, A. Maas, and T. Mendes, *Phys. Rev.* **D74** (2006) 014503, [arXiv:hep-lat/0605011](#).
- [58] E. M. Ilgenfritz, M. Müller-Preussker, A. Sternbeck, A. Schiller, and I. L. Bogolubsky, *Braz. J. Phys.* **37** (2007) 193, [arXiv:hep-lat/0609043](#).
- [59] W. Schleifenbaum, A. Maas, J. Wambach, and R. Alkofer, *Phys. Rev.* **D72** (2005) 014017, [hep-ph/0411052](#).
- [60] M. Q. Huber and M. Mitter, *Comput.Phys.Commun.* (2012) , [arXiv:1112.5622 \[hep-th\]](#).
- [61] J. C. Bloch, *Few Body Syst.* **33** (2003) 111–152, [arXiv:hep-ph/0303125 \[hep-ph\]](#).
- [62] R. Alkofer, M. Q. Huber, V. Mader, and A. Windisch, *PoS QCD-TNT-II* (2011) 003, [arXiv:1112.6173 \[hep-th\]](#).
- [63] D. Binosi and L. Theussl, *Comput.Phys.Commun.* **161** (2004) 76–86, [arXiv:hep-ph/0309015 \[hep-ph\]](#).